

**Title Page**

**Mechanisms and Predictions of Drug-Drug Interactions of the Hepatitis C Virus 3-Direct Acting  
Antiviral (3D) Regimen: Paritaprevir/Ritonavir, Ombitasvir and Dasabuvir**

Mohamad Shebley, Jinrong Liu, Olga Kavetskaia, Jens Sydor, Sonia M. de Morais, Volker Fischer,  
Marjoleen J.M.A. Nijsen, Daniel A.J. Bow

Drug Metabolism, Pharmacokinetics and Bioanalysis (M.S., J.L., O.K., J.S., S.M.D.M., V.F., M.J.M.A.N.,  
D.A.J.B.), Clinical Pharmacology and Pharmacometrics (M.S.), AbbVie Inc., North Chicago, Illinois

## Running Title Page

Running Title: DDI mechanisms and predictions of the HCV 3D regimen

Corresponding author: Mohamad Shebley, Department of Clinical Pharmacology and Pharmacometrics, AbbVie Inc., 1 N. Waukegan Rd., AP31-3, North Chicago, Illinois, 60064, USA; tel: (847) 938-3662; email: [mohamad.shebley@abbvie.com](mailto:mohamad.shebley@abbvie.com)

Number of text pages: 19

Number of tables: 5

Number of Supplemental tables: 9

Number of figures: 1

Number of Supplemental Figures: 3

Number of references: 34

Number of words in Abstract: 250 words

Number of words in Introduction: 396 words

Number of words in Discussion: 1,900 words

Abbreviations: 3D, AbbVie's three direct acting antiviral regimen; AUCR, AUC ratio of substrate with perpetrator relative to control; CYP, cytochrome P450; DAA, direct acting antiviral; DDI, drug-drug interaction; HCV, hepatitis C virus

## Abstract

To assess drug-drug interaction (DDI) potential for the 3 direct-acting antiviral (3D) regimen of ombitasvir, dasabuvir and paritaprevir, *in vitro* studies profiled drug metabolizing enzyme and transporter interactions. Using mechanistic static and dynamic models, DDI potential was predicted for CYP3A, CYP2C8, UGT1A1, OATP1B1/1B3, BCRP and P-gp. Perpetrator static model DDI predictions for metabolizing enzymes were within 2-fold of the clinical observations but for drug transporters, additional PBPK modeling was necessary to achieve the same. When assessing perpetrator interactions, ritonavir is responsible for the strong increase in exposure of sensitive CYP3A substrates while paritaprevir (OATP1B1/1B3 inhibitor) increases greatly the exposure of sensitive OATP1B1/1B3 substrates. The 3D regimen drugs are UGT1A1 inhibitors and are predicted to increase moderately plasma exposure of sensitive UGT1A1 substrates. Paritaprevir, ritonavir and dasabuvir are BCRP inhibitors. Victim DDI predictions were qualitatively in line with the clinical observations. Plasma exposures of the 3D regimen were reduced by strong CYP3A inducers (paritaprevir and ritonavir; major CYP3A substrates), but not impacted by strong CYP3A4 inhibitors since ritonavir (CYP3A inhibitor) is already present in the regimen. Strong CYP2C8 inhibitors increase plasma exposure of dasabuvir (major CYP2C8 substrate), OATP1B1/1B3 inhibitors increase the plasma exposure of paritaprevir (OATP1B1/1B3 substrate), and P-gp or BCRP inhibitors (all compounds are substrates of P-gp and/or BCRP) increase plasma exposure of the 3D regimen. Overall, the comprehensive mechanistic assessment of compound disposition along with mechanistic and PBPK approaches to predict victim and perpetrator DDI liability, may enable better clinical management of non-studied drug combinations with the 3D regimen.

## Introduction

It is estimated that 170 million people worldwide are chronically infected with hepatitis C virus (HCV) (WHO, 2011). Recently, orally available direct-acting antiviral (DAA) agents and compounds in clinical development have emerged to cure HCV infected patients (Burger et al., 2013). Successful HCV therapies may require a combination of DAAs similar to HIV regimens, and in some cases the use of pharmacokinetic (PK) enhancers such as ritonavir may be needed. Approved HCV protease inhibitors such as telaprevir, boseprevir and simeprevir, and polymerase inhibitors such as the prodrug sofosbuvir are substrates and inhibitors of drug metabolizing enzymes and transporters, which are regularly involved in DDIs (Khalilieh et al., 2015; Kirby et al., 2015; Maasoumy et al., 2013). AbbVie's 3D regimen is an all-oral interferon-free combination of the protease inhibitor paritaprevir (identified by AbbVie and Enanta) co-formulated with ritonavir as a systemic PK enhancer and the NS5A inhibitor ombitasvir, plus the non-nucleoside polymerase inhibitor dasabuvir with and without ribavirin (Feld et al., 2014). Frequently, HCV patients are taking concomitant medications to treat conditions related to HCV or other co-morbidities (Burger et al., 2013), leading to a poly-pharmacy with potential for complex DDIs, which in turn becomes an important consideration for physicians when using the most appropriate DAA regimen (Soriano et al., 2015). These DDIs mainly lead to systemic PK changes which could impact the pharmacodynamic response and/or safety of concomitantly administered drugs, such as in the case of HIV-HCV co-infected and post-transplant patients, and in some cases require dose adjustment or therapeutic monitoring of the affected medication(s).

Similar to HIV treatments, it is challenging to predict or extrapolate complex DDIs for a given combination in the absence of data from DDI clinical trials. In addition, it is not feasible to study all drug combinations in dedicated healthy volunteer trials to assess DDI for every drug and mechanism, and with all possible concomitant medications. Therefore predictive non-clinical models are essential to aid in our understanding of the complex enzymes and transporters interplay for each drug within the 3D regimen. To assess DDI potential against drug metabolizing enzymes and drug transporters, the ADME properties for each drug in the 3D regimen (including a major circulating metabolite of dasabuvir, M1) were

determined in the context of the 3D regimen clinical exposure. Predictions were used to not only inform clinical DDI trial design but also offer mechanistic explanation for observed clinical DDIs.

## Materials and Methods

### Metabolism Studies

#### CYP and UGT inhibition

Cytochrome P450 (CYP) and uridine-diphosphate glucuronosyltransferase (UGT) reversible inhibition was determined by measuring the extent of enzyme probe substrate conversion to the corresponding specific metabolite in human liver microsomes (HLMs). Known inhibitors were included as positive controls for each enzyme isoform. Test compounds were incubated at concentrations up to 30  $\mu$ M for all CYP isoforms (100  $\mu$ M for CYP2B6), and up to 50  $\mu$ M for all UGTs). The probe substrate concentration for each CYP or UGT isoform was close to the previously reported  $K_m$  values and assay incubations (pH 7.4) contained NADPH (1 mM) in phosphate buffer (50 mM) (CYP isoforms) or UDPGA (5 mM) in Tris-HCL buffer (50 mM) with magnesium chloride (10 mM) (UGT isoforms). Specific assay conditions are included in the Supplemental Table 1 and 2. Sample analysis of various enzyme incubations was performed by liquid chromatography mass spectrometry (LCMS) using synthetic standards of metabolites with internal standards. For time-dependent inhibition (TDI) studies, the primary incubations consisted of 1 mg/mL HLM with 10 and 50  $\mu$ M test compound or positive controls (known mechanism-based inactivators for each CYP isoform), 1 mM NADPH in potassium phosphate buffer (100 mM) at pH 7.4, incubated at 37°C for 0 and t1 (10-30 minutes, see Supplemental Table 3). Residual enzyme activity was determined using the CYP specific metabolite as a marker of activity activities. TDI potential was measured by calculating the difference in the extent of conversion of each CYP substrate to its corresponding metabolite (0 min to t1). Probe substrates were used in excess amount concentrations >4-fold of  $K_m$ ) for each CYP isoform. Specific TDI assay conditions are included in Supplemental Table 3.

#### CYP induction

CYP induction was assessed in human hepatocytes from three donors, two females and one male. Cryopreserved hepatocytes were thawed (37 °C), centrifuged (10 minutes, 100 x g; CHRM recovery

medium (Life Technologies, Inc., Rockville, MD, USA) and re-suspended in William's E medium (without phenol red) (WEM) supplemented with dexamethasone (0.1  $\mu$ M), insulin (0.0001%), penicillin and streptomycin (100 IU/mL), and new born calf serum (5%). Hepatocyte viability was assessed by Trypan blue exclusion and cells seeded in collagen-coated 96-well plates (~0.8-0.9 million cells/mL). Cells were incubated at 37°C (95% air/5% CO<sub>2</sub>) for 4-5 hours to allow hepatocytes to attach and then overlaid with Geltrex™ (Life Technologies) (0.35 mg/mL). Cells were incubated overnight and then treated with test compounds (0.1 – 10  $\mu$ M) or positive controls (50  $\mu$ M omeprazole;CYP1A2, 50  $\mu$ M phenytoin;CYP2B6, 10  $\mu$ M rifampin;CYP3A4) in serum-free incubation medium (WEM plus hepatocyte maintenance supplement pack; ThermoFisher Scientific) with 0.1% DMSO for 48 hours (medium changed daily). At the end of the incubation cell viability was assessed, according to manufacturer instructions for PrestoBlue™ cell viability reagent (Life Technologies) before RNA was isolated using MagMAX™ Express 96 RNA Isolation System (Life Technologies). CYP mRNA expression for CYP1A2, 3A4 and 2B6 was assessed by RT-PCR (ViiA™ 7 Real-Time PCR System (ThermoFisher Scientific) using the TaqMan EZ RT-PCR kit and standard probe/primer sets for each CYP isoform (Supplemental Table 4). Human 28S was used as an internal control to account for any variability in RNA levels. Induction was assessed by comparing CYP mRNA fold-change between test compound treated and vehicle (0.1% DMSO) control cells and % induction of the positive controls of CYP mRNA by the test articles compared to the vehicle control (0.1% DMSO) and % of induction of the positive controls.

#### CYP phenotyping

Each compound (1-5  $\mu$ M with tritium radiolabel tracer) was incubated with a panel of CYP (1A2, 2B6, 2C8, 2C9, 2D6, 3A4, 3A5) Supersomes (BD Gentest, Woburn, MA) at 100 nmol/mL in phosphate buffer (100 mM, pH 7.4) in triplicate. To monitor formation of metabolites using radio-detection coupled with HPLC. Reactions were supplemented with NADPH (1 mM) and conducted at 37°C for 45 minutes, and terminated by the addition of organic solvent (acetonitrile/methanol (v/v 1:1)). The samples were centrifuged (4000 rpm, 30 minutes) and reaction supernatant was analyzed. Ritonavir was not tested in this study; therefore, previous results were reported (Kumar et al., 1996). If more than one metabolizing enzyme was identified from the Supersomes studies, follow-up incubations with HLMs in presence of known inhibitors of specific CYP isoforms were conducted. Only dasabuvir was studied with specific inhibitors

(ketoconazole, CYP3A, 0.03-1  $\mu\text{M}$ ; quercetin, CYP2C8, 0.5-45  $\mu\text{M}$ ); incubations of dasabuvir (0.25  $\mu\text{M}$ ) with HLMs (0.5 mg/mL) at 37°C for 60 min. Reactions were terminated and analyzed as described above. The contribution of each enzyme was assessed qualitatively based on detection of metabolites peaks from incubations. Contributions of each CYP was estimated based on observed turnover in the Supersomes incubations for all compounds, except for dasabuvir where final CYP contributions was calculated based on the chemical inhibition results with selective CYP3A and 2C8 inhibitors.

## Transporter Studies

### Uptake Transporters

Substrate studies: human Embryonic Kidney (HEK) cells stably expressing Organic anion transporting polypeptide (OATP) 1B1 or 1B3 (obtained from Prof. Dietrich Keppler, German Cancer Research Center (DKFZ), Heidelberg, Germany) or Organic anion transporter (OAT)1, OAT3, Organic Cation Transporter (OCT) 1, OCT2, Multi-drug and toxin extrusion protein (MATE)1 or MATE2K (obtained from Kathleen M. Giacomini, Department of Biopharmaceutical sciences, School of Pharmacy, University of California, San Francisco) were used for substrate and/or inhibition evaluation for each of the compounds in the 3D regimen. OATP1B3 used in these studies has a mutation at amino acid 112 (serine to alanine). This mutated form has been shown to exhibit the same substrate specificity as the native form of OATP1B3 (Fahrmayr et al., 2010).

Assays were performed as previously described (Chiou et al., 2014; Kikuchi et al., 2013) with incubation time points optimized for each of the individual transporters. Uptake of reference substrates (Para-aminohippuric acid (PAH), estrone sulfate (ES), and 1-methyl-4-phenylpyridinium (MPP<sup>+</sup>) were used for OAT1, OAT3, and OCT2/MATE1/MATE2K, respectively. Substrate uptake studies for each compound in the 3D regimen were conducted at multiple concentrations. If active uptake was observed, uptake kinetics ( $K_M$  and  $V_{max}$ ) were determined by plotting the rate of initial uptake ( $V_o$ , pmol/minute/mg protein) against the compound concentrations ( $\mu\text{M}$ ) using the Michaelis-Menten equation.  $K_M$  and  $V_{max}$  were determined by using non-linear regression curve-fitting in GraphPad® Prism.

Inhibition studies: for each of the transporters, uptake inhibition was determined by incubations in the presence of increasing concentrations of each of the test compounds.  $IC_{50}$  values for inhibition (if calculated) were determined by using non-linear regression curve-fitting in GraphPad® Prism.

### Efflux Transporters

Substrate studies: *In vitro* efflux substrate assays were performed using MDCKII cells stably expressing P-glycoprotein (P-gp) or Breast Cancer Resistance Protein (BCRP). The cell lines were originally obtained from Professor Piet Borst (Netherlands Cancer Institute, Amsterdam, Netherlands) and modified to knockout the expression of endogenous canine P-gp (Gartzke and Fricker, 2014). Cells were grown to confluence on Millicell 96 Cell Culture Plate polycarbonate filters and substrate assays for each of the compounds in the 3D regimen were conducted as outlined in (Gartzke and Fricker, 2014). For ombitasvir efflux studies, assay conditions were modified to include 1% BSA (w/v) in the incubation medium to reduce non-specific binding.

Inhibition studies: P-gp and BCRP efflux inhibition was determined by incubating in the presence of increasing concentrations of each of the DAAs. Efflux ratios were obtained according to the following formula:  $\text{Efflux Ratio} = P_{\text{app B-to-A}}/P_{\text{app A-to-B}}$ .  $IC_{50}$  values were determined in GraphPad® Prism, with the equation:  $\log(\text{inhibitor})$  vs. response – variable slope.

For membrane vesicle studies, assays were conducted according to the kit protocol (GenoMembrane) with minor modifications. BCRP- or MRP2-expressing or control membrane vesicles were pre-incubated in a transport buffer A at 37°C for five min, then rapidly mixed with assay mixture containing 4 mM ATP or AMP and the transporter probe substrate (100  $\mu\text{M}$  [ $^3\text{H}$ ]methotrexate (MTX; 10  $\mu\text{Ci}/\text{mL}$ ) for BCRP or 50  $\mu\text{M}$  [ $^3\text{H}$ ]estradiol 17- $\beta$ -glucuronide (E217 $\beta$ G; 4  $\mu\text{Ci}/\text{mL}$ ) for MRP2) in the presence or absence of a known inhibitor or test compound for 2-3 minutes. Transport was terminated by addition of ice-cold wash buffer. The incubation mixture was filtered through a glass fiber filter plate and filters washed with wash buffer. Radioactivity associated with each filter and incubation buffers was determined using a Micro- $\beta$ 2 counter. ATP-dependent transport was calculated by subtracting the values obtained in the presence of AMP from those in the presence of ATP. Transporter-specific transport was calculated by subtracting the ATP-dependent MTX uptake in control vesicles from the ATP-dependent MTX uptake in the transporter-



expressing vesicles. IC<sub>50</sub> values were obtained by examining its inhibitory effect on the ATP-dependent transport of reference substrate assuming competitive inhibition. Fitting was performed by the nonlinear least-squares method using GraphPad Prism (Ver. 5.04).

### Predictions of CYP and UGT Interactions

Predictions of potential DDI of the 3D regimen via CYP inhibition were made according to the U.S. FDA 2012 draft guidance for industry on drug interaction studies (FDA, 2012), and following the recommendations in Figure 4 of the guidance using the mechanistic static model for reversible inhibition:

$$AUCR = \left( \frac{1}{[A_g] \times (1 - F_g) + F_g} \right) \times \left( \frac{1}{[A_h] \times f_m + (1 - f_m)} \right) \quad \text{(Equation 1)}$$

$$\text{Gut: } A_g = \frac{1}{1 + \frac{[I]_g}{K_i}} \quad \text{where } [I]_g = F_a \times K_a \times \text{Dose}/Q_{en}$$

$$\text{Liver: } A_h = \frac{1}{1 + \frac{[I]_h}{K_i}} \quad \text{where } [I]_h = f_{u,b} \times ([I]_{max,b} + F_a \times K_a \times \text{Dose}/Q_h)$$

$$cAUCR = \left( \frac{1}{[A_{g,comb}] \times (1 - F_g) + F_g} \right) \times \left( \frac{1}{[A_{h,comb}] \times f_m + (1 - f_m)} \right) \quad \text{(Equation 2)}$$

$$\text{Gut: } A_{g,comb} = \frac{1}{1 + \sum \frac{[I]_{g,drug1}}{K_{i,drug1}} + \frac{[I]_{g,drug2}}{K_{i,drug2}} + \dots}$$

$$\text{Liver: } A_{h,comb} = \frac{1}{1 + \sum \frac{[I]_{h,drug1}}{K_{i,drug1}} + \frac{[I]_{h,drug2}}{K_{i,drug2}} + \dots}$$

AUCR is the ratio of victim drug AUC in presence of interacting drug relative to control; cAUCR is a combination AUCR for a victim drug based on summing together ratios of inhibitor *in vivo* concentration to *in vitro* K<sub>i</sub> in gut or liver of all drugs within 3D regimen for a given CYP or UGT isoform; subscripts “h” and “g” denote liver and gut, respectively; *comb* refers to parameters calculated for the combination; F<sub>a</sub> is the fraction absorbed after oral administration; K<sub>a</sub> is the first order absorption rate constant *in vivo*; Q<sub>en</sub> and Q<sub>h</sub> are blood flow through enterocytes (18 L/hr/70 kg) and hepatic blood flow (97 L/hr/70 kg), respectively; f<sub>m</sub> is the fraction of systemic clearance of the substrate mediated by the CYP enzyme that is subject to

inhibition;  $[I]_{\max,b}$  is maximum systemic blood concentration;  $K_i$  is the *in vitro* enzyme inhibition constant (FDA, 2012). For M1 only, prediction of UGT inhibition was also based on the ratio ( $R_1$ ) of unbound  $C_{\max}$  to *in vitro* enzyme  $K_i$ .

Assumptions:  $f_m$  of CYP probe substrates is assumed to be 0.99 (represents an upper estimate of the enzyme contribution, (Brown et al., 2005),  $F_g$  of midazolam as a CYP3A probe substrate was assumed to be 0.53 (Simcyp V14.1),  $K_a$  values used for each drug were previously reported (Mensing et al., 2016).

All drug parameters used in metabolism-based perpetrator DDI predictions are summarized in Table 2.

### Predictions of Transporter Interactions

DDI predictions for efflux, hepatic uptake, and renal transporter inhibition decision trees, in the US FDA 2012 draft guidance for industry on drug interaction studies (FDA, 2012).

For predictions of efflux transport inhibition and hepatic uptake inhibition, following equations were used:

$$[I]_1/IC_{50} \text{ (or } K_i) \geq 0.1 \quad \text{(Equation 3)}$$

$$[I]_2/IC_{50} \text{ (or } K_i) \geq 10 \quad \text{(Equation 4)}$$

Where  $[I]_1$  represents the mean steady-state total (free and bound)  $C_{\max}$  following administration of the highest proposed clinical dose.  $[I]_2 = \text{Dose of inhibitor (in mol)}/250 \text{ mL}$  (if  $IC_{50}$  is in a molar unit) (FDA, 2012).

$$R\text{-value} = 1 + (f_u \times I_{in,max}/IC_{50}) \quad \text{(Equation 5)}$$

Where R-value is the ratio of victim drug AUC with inhibitor relative to AUC without inhibitor,  $I_{in,max}$  is the estimated maximum inhibitor concentration at the inlet to the liver:

$$I_{in,max} = C_{max} + (K_a \times Dose \times F_a F_g / Q_h) \quad \text{(Equation 6)}$$

$C_{max}$  is the maximum systemic plasma concentration of inhibitor; Dose is the inhibitor dose;  $F_a F_g$  is the fraction of the dose of inhibitor which is absorbed;  $K_a$  is the absorption rate constant of the inhibitor and  $Q_h$  is the estimated hepatic blood flow (1500-1600 mL/min).

For renal transporters, predictions were based on  $C_{max,u}/IC_{50}$  with cutoff of 0.1 (FDA, 2012).

All drug parameters used in transporter-based perpetrator DDI predictions are summarized in Table 2.

### Physiologically-Based Pharmacokinetic (PBPK) modeling

Pravastatin, rosuvastatin and digoxin PBPK substrate files were used directly from the default 'Substrate' library of Simcyp v14.1. These model files were verified against clinical data and published previously (Jamei et al., 2014; Neuhoff et al., 2013; Varma et al., 2012). PBPK models for the 3D regimen as perpetrators were constructed using a combination of 'top-down' and 'bottom-up' approaches in Simcyp v14.1, using clinical PK data for paritaprevir, ritonavir and dasabuvir, and in vitro transporter inhibition data. Ombitasvir was not included in the PBPK model development process or the simulations as transporter inhibition was not observed in vitro. Physical-chemical properties and observed oral clearance (CL/F) values from clinical PK studies for each drug were entered into Simcyp, and volume of distribution ( $V_{ss}$ ) was estimated using a minimal PBPK model (Rowland Yeo et al., 2010) with user input values and optimized parameter estimates (details in Supplemental Tables 5-7) to fit the PK profile of each drug. The disposition and elimination mechanisms of each drug were not assigned in the PBPK models because the models were intended to be used as perpetrators only. Absorption parameters  $f_a$  and  $k_a$  were estimated using a top-down approach to match the  $C_{max}$  and  $T_{max}$  of each drug. Distribution parameters  $V_{ss}$ , single adjusting compartment (SAC) and intercompartmental clearance (Q) were estimated using a top-down approach to match the observed shape of the PK curves for each drug. As paritaprevir is a substrate for hepatic uptake transporters (Table 1), the liver-to-plasma ratio was assumed to be higher than unity. The paritaprevir final PBPK model was optimized by applying parameter estimation to the liver-to-plasma partition coefficient ( $K_p$ ) and hepatic uptake factor of paritaprevir using clinical PK data (Supplemental Table 5). Validation of the 3D PBPK models was achieved by matching simulations results with observed clinical PK profiles of the 3D regimen. For DDI simulations with the 3D

regimen, *in vitro* transporters  $IC_{50}$  values for each drug were used to predict the observed DDIs by the final PBPK models. For all DDI simulations, virtual trial designs (using a single population representative) in Simcyp were matched with clinical study designs. For pravastatin and rosuvastatin, 150 mg QD paritaprevir with 100 mg QD ritonavir and 400 mg BID dasabuvir were simulated for 14 days with 10 mg QD pravastatin or 5 mg QD rosuvastatin under fed conditions. For digoxin, 0.5 mg single dose of digoxin was administered on day 15 following 150 mg QD paritaprevir with 100 mg QD ritonavir and 400 mg BID dasabuvir for 20 days under fed conditions. For comparison with the predicted DDI ratios, published clinical  $C_{max}$  and AUC geometric mean ratios of the victim drugs were used. (Menon et al., 2015).

## Results

### Metabolism data

Perpetrator profile - *in vitro* inhibition data for CYPs and UGTs by paritaprevir, ritonavir, ombitasvir, and dasabuvir and its major metabolite M1 are summarized in Supplemental Table 8. Ritonavir UGT inhibition was not studied; the literature value for UGT1A1 inhibition is reported in Supplemental Table 8 (Zhou et al., 2011). For reversible inhibition of CYPs, paritaprevir and ombitasvir inhibited CYP2C8. Ritonavir inhibited CYP2B6, CYP2C8/9/19, CYP2D6, and CYP3A. Dasabuvir, but not M1, inhibited CYP2B6, CYP2C8/9/19, and CYP2D6 with relatively much weaker potency compared to ritonavir. All drugs in the 3D regimen inhibited UGT1A1. Paritaprevir, dasabuvir, and M1 inhibited UGT1A4, paritaprevir and dasabuvir inhibited UGT1A6, dasabuvir and M1 inhibited UGT1A9, and dasabuvir only inhibited UGT2B7.

For TDI of CYPs, ritonavir is a potent inhibitor of CYP3A4 (20-77% pre-incubation effect at 0.1 and 1  $\mu$ M, respectively) while paritaprevir and M1 exhibited minimal TDI on CYP3A4 (~10-15% pre-incubation effect at 10 and 50  $\mu$ M, respectively). TDI parameters such as the inhibition constant  $K_i$  and the first order rate of inactivation constant  $k_{inact}$ , were not determined for paritaprevir and M1 due to the weak TDI observed *in vitro*, and were not obtainable for ritonavir due to the overlapping reversible inhibition potency with the TDI effect *in vitro*. Therefore TDI based predictions using static models were not attempted.

In human primary hepatocytes, ritonavir potently induced CYP3A4 mRNA (83% of rifampin response, at 10  $\mu$ M), and paritaprevir showed weaker induction (30% of rifampin response, at 10  $\mu$ M) (Supplemental Table 9).

Victim profile - recombinant CYP phenotyping studies indicated that paritaprevir, ombitasvir, and M1 are predominantly metabolized by CYP3A4 with no metabolism observed by other CYPs. There was some turnover of paritaprevir in CYP3A5 incubations; however the contribution of CYP3A5 is considered negligible since its intestinal and hepatic expression is relatively much lower compared to CYP3A4. Although ombitasvir and M1 appear predominately metabolized by CYP3A4 *in vitro*, ombitasvir is primarily metabolized by non-CYP amide hydrolysis pathways *in vivo* (little to negligible contribution by CYP3A4) and M1 is eliminated *in vivo* (Shen et al., 2016a) primarily unchanged via the hepatobiliary and urinary routes (minimal metabolism via CYPs and direct glucuronidation). Dasabuvir was metabolized predominantly by CYP2C8 with partial metabolism by CYP3A (Table 1) based on results from the chemical inhibition study.

### Transporters data

Perpetrator profile - *In vitro* inhibition data for efflux and uptake transporters are summarized in Supplemental Table 8. Paritaprevir, ritonavir, dasabuvir, and M1 inhibited P-gp and BCRP, and the hepatic uptake transporters OATP1B1 and OATP1B3. Ritonavir inhibited OCT1. Renal transporters, OAT1 and OAT3, were inhibited by paritaprevir and ritonavir. Ritonavir and M1 inhibited MATE1 and MATE2K, and paritaprevir inhibited MATE2K.

Victim profile - All drugs in 3D regimen and M1 are P-gp substrates, while only paritaprevir, dasabuvir and M1 are BCRP substrates. Paritaprevir and M1 are substrates for the hepatic uptake transporters, OATP1B1 and OATP1B3, and M1 is a substrate for OCT1 (Table 1). As paritaprevir, ritonavir, ombitasvir, and dasabuvir have minimal renal elimination, *in vitro* renal transport substrate studies were not conducted.

### Metabolism-mediated DDI predictions

For better understanding of the overall effects and predicted DDIs with the 3D regimen, individual and combined predictions were determined and explained in the context of a combination drug regimen. Predictions of metabolism-based DDI potential of the 3D regimen were based on clinical doses, plasma exposures and PK parameters (Table 2), and using the U.S. FDA recommended basic and mechanistic static models (Equation 1, Materials and Methods) (FDA, 2012) with modification to predict the combination effect (Equation 2, Materials and Methods).

Inhibition potential - Ritonavir had the highest predicted AUCR with CYP3A4 (AUCR = 38) (Table 3). In a clinical study with the 3D regimen and the CYP3A sensitive substrate tacrolimus, ritonavir caused a strong interaction (observed AUCR = 57) (AbbVie, 2014), consistent with the predicted AUCR of 28 and within 2-fold. The predicted CYP2C9 individual AUCR and cAUCR values for dasabuvir and ritonavir were below the FDA cutoff of 1.25 (Table 3), suggesting a low inhibition potential. Clinical interaction with warfarin as a CYP2C9 probe substrate resulted in AUCR of 0.9 (Table 3) consistent with predicted AUCR within 1.3-fold, and confirming the absence of clinically significant CYP2C9 interaction by the 3D regimen (Menon et al., 2015). The predicted CYP2C19 cAUCR was consistent with the clinical results of omeprazole (CYP2C19 substrate), where clinical inhibition of CYP2C19 following co-administration of the 3D regimen was not observed (observed AUCR = 0.62) (Menon et al., 2015). In this clinical study, decreased exposure of omeprazole following co-administration with 3D regimen can be explained by a net induction of CYP2C19 by ritonavir which was reported previously (Yeh et al., 2006).

All compounds in the 3D regimen, including the M1 metabolite of dasabuvir, inhibit UGT1A1 *in vitro* with a range of potencies (Supplemental Table 8). Based on the same approach to predict reversible CYP inhibition DDI using the mechanistic static model described above, only dasabuvir had a relatively higher predicted AUCR (1.06) but still below the cutoff of 1.25, suggesting a remote potential for interaction with co-administered substrates of UGT1A1, while the cAUCR (1.20) predicted a weak interaction (Table 3). The predicted cAUCR of 1.20 was within 2-fold of a moderate and not clinically relevant observed AUCR of 2.4 with raltegravir (substrate of UGT1A1) (Menon et al., 2015).

Victim potential - Based on *in vitro* studies all drugs in the 3D regimen are CYP3A4 substrates with varying degrees of sensitivity and extent of contribution to their elimination (Table 1). The significant

contribution of CYP3A4 to elimination of paritaprevir was confirmed in clinical studies following co-administration with ritonavir where paritaprevir exposure was markedly increased (Menon et al., 2015). While within 3D regimen, only a moderate (observed AUCR = ~2) clinical interaction with ketoconazole (potent CYP3A4/P-gp inhibitor) was observed due to the presence of co-formulated ritonavir (Menon et al., 2015).

Dasabuvir is predominantly metabolized by CYP2C8 (~60%) and to a lesser extent by CYP3A4 (30%) based on *in vitro* data from incubations with selective CYP2C8 and CYP3A inhibitors. A clinical study with dasabuvir and the potent CYP2C8 inhibitor gemfibrozil confirmed the significant contribution of CYP2C8 (observed AUCR ~11), while the minor contribution of CYP3A4 (observed AUCR < 2) was confirmed in a clinical study with ketoconazole co-administration (Menon et al., 2015).

Although CYP3A4 appeared to metabolize ombitasvir *in vitro*, the extent of metabolism is limited and contribution of CYP3A4 to the overall elimination of ombitasvir is minimal due to the predominant amide hydrolysis pathway and the presence of co-administered ritonavir within the 3D regimen, consistent with the absence of interaction with ketoconazole (Menon et al., 2015).

Based on *in vitro* metabolism data of predominant role of CYP3A, plasma exposures of all drugs within the 3D regimes were predicted to be significantly affected by strong CYP3A inducers. A significant decrease (>30%) in paritaprevir, ritonavir, dasabuvir, and ombitasvir systemic exposures was observed following co-administration with the strong CYP3A inducer carbamazepine (Menon et al., 2015).

### **Transporter-mediated DDI predictions**

Predictions of transporters-based DDI of the 3D regimen were based on *in vitro* IC<sub>50</sub> values, clinical doses and plasma exposures (Table 2), and the U.S. FDA recommended basic and mechanistic static models (equations 2-5, Materials and Methods) (FDA, 2012).

Inhibition potential - Inhibition of intestinal efflux transporters (P-gp, BCRP) was predicted to be possible ( $[I_2]/IC_{50}$  values >10) for paritaprevir, ritonavir, and dasabuvir but not likely for ombitasvir, Table 4a. Inhibition of efflux transporters at other tissue sites (i.e. liver and kidney) was predicted for P-gp by

ritonavir ( $[I_1]/IC_{50}$  value 6.3) and for BCRP by paritaprevir ( $[I_1]/IC_{50}$  values 3.2), while dasabuvir predictions were slightly above the cutoff point of 0.1, Table 4a. In clinical studies, a small increase (~16%) in systemic exposure of digoxin was observed with the 3D regimen (Menon et al., 2015). In efforts to further evaluate the transporters-based DDI predictions of the 3D regimen, PBPK modeling was employed. The PBPK models of paritaprevir, ritonavir and dasabuvir were developed using a combined bottom-up (in vitro transporters  $IC_{50}$  values) and top-down (clinical PK parameters) approach. The developed models were calibrated using clinical PK data, where absorption and distribution parameters were optimized for paritaprevir, ritonavir and dasabuvir to fit each drug's clinical PK profile and parameters. The final models were in good agreement with the clinical data (Supplemental Figures 1-3) and were simulated in combination during all DDI trial simulations. PBPK simulations of the 3D regimen at steady state with a single dose of digoxin, a P-gp substrate, on day 15 resulted in negligible changes in digoxin exposure. Digoxin predicted  $C_{max}$  ratio of 1.19 and AUC ratio of 1.20 following co-administration with the 3D regimen were within 1.25-fold of clinical results (Table 4b). Effects of the 3D regimen on BCRP was simulated using rosuvastatin as a probe substrate and the predicted  $C_{max}$  ratio of 3.4 and AUC ratio of 2.4 were within 2-fold of the clinical results (Table 4b).

For hepatic uptake transporters, R-values of OATP1B1 and 1B3 by paritaprevir (R-values 2.6 and 3.9, respectively; Table 4a) suggested a moderate DDI but were quantitatively over-predictive of the clinical interaction with the OATP1B1/1B3 substrate pravastatin (observed AUCR 1.82) and the mixed OATP1B1/1B3 and BCRP substrate rosuvastatin (observed AUC 2.59) systemic exposures (Menon et al., 2015). PBPK simulations of the 3D regimen drugs as perpetrators with pravastatin and rosuvastatin significantly improved the predicted AUC ratios and provided an advantage in predicting  $C_{max}$  ratios within the 2-fold acceptance criteria (Table 4b) compared to the R-value static predictions. Although PBPK-based predictions were closer to the observed data compared to static models, there was a slight under prediction of rosuvastatin  $C_{max}$  ratio compared to clinical observation (predicted 3.4 vs. observed 7.1), therefore sensitivity analysis on intestinal BCRP  $IC_{50}$  values for paritaprevir, ritonavir and dasabuvir was employed. The additional PBPK sensitivity analysis simulations revealed that only paritaprevir  $IC_{50}$  was sensitive to intestinal BCRP interaction, where a threefold decrease in paritaprevir  $IC_{50}$  resulted in an improvement in the predicted  $C_{max}$  ratio of 4.10 and AUC ratio of 2.55. Further decrease (60-600 fold) in



paritaprevir BCRP  $IC_{50}$  value increased the  $C_{max}$  ratio up to a maximum of 5-fold, with a consistent under prediction of the observed value ( $C_{max}$  ratio 7.1-fold).

For renal transporters, unbound plasma concentrations of the 3D regimen were predicted to be insufficient to clinically inhibit OAT1, OAT3, OCT2 or MATE1 and MATE2K. Consistently, clinical interaction with the OAT1 substrate tenofovir and OCT2 substrate metformin following co-administration with the 3D regimen was not observed (Menon et al., 2014; Menon et al., 2015; Polepally et al., 2016).

Victim potential - As victims of transporters, paritaprevir, dasabuvir, and M1 are substrates for P gp and BCRP, while ritonavir and ombitasvir are substrates for P-gp only (Table 1). Although ketoconazole *in vivo* inhibitory contribution on efflux transporters versus CYP3A is difficult to discern, co-administration increased exposure of paritaprevir, ritonavir and dasabuvir, while ombitasvir was not affected (Menon et al., 2015).

Paritaprevir and M1 are substrates for OATP1B1 and OATP1B3 (Table 1) *in vitro*, and strong inhibitors were expected to increase paritaprevir or M1 systemic exposure. The systemic exposure of paritaprevir but not M1, was sensitive to OATP inhibition following co-administration with the OATP inhibitors, atazanavir and cyclosporine (Menon et al., 2015).

## Discussion

In this study, *in vitro* metabolism and transporter interactions for paritaprevir, ritonavir, ombitasvir, dasabuvir and M1 (a metabolite of dasabuvir) were characterized and extrapolated using static and dynamic DDI models. Clinical DDI studies were conducted during the development of the 3D regimen to evaluate interactions with CYPs, UGTs, and drug transporters. The results from those DDI trials were in agreement with the predictions using *in vitro* data (Tables 1, 3, 4).

Perpetrator profile: All CYP-mediated DDI predictions using static mechanistic models were within 2-fold of the observed data. Ritonavir was responsible for the majority of CYP-mediated interactions as a strong inhibitor of CYP3A and moderate inducer of CYP2C19 (Table 5). For UGTs, the cAUCR approach was able to predict a potential inhibitory interaction, consistent with the observed DDI with a UGT1A1

substrate raltegravir (Menon et al., 2015) (Table 5). The proposed cAUCR is a simplistic approach for predicting effects of combination drugs on one mechanism; however, a similar approach for predicting metabolite-based DDI (Templeton et al.2016) was recently reported and may be justified for predicting drug combination DDIs. Overall, metabolism-based perpetrator predictions were in good quantitative agreement with clinical data when the 2-fold criterion was applied.

Paritaprevir, ritonavir and dasabuvir were predicted to inhibit intestinal P-gp, while only ritonavir and dasabuvir were predicted to inhibit P-gp in liver and kidney (Table 4a). Only a minimal increase in the exposure (similar magnitude increase for both  $C_{max}$  and AUC)of digoxin was observed suggesting that this interaction may have only occurred in the intestine. However, previous reports have suggested the lack of sensitivity of digoxin to intestinal P-gp inhibition (Shi et al., 2011; Nader et al., 2013) and over-prediction of the observed DDI by the static models may be explained in part by some of the assumptions in the calculations. For example, the static model assumes that the compound/s are fully soluble in 250 mL, and unlike the PBPK model, static modeling does not account for parameters such as permeability, transit time in the intestine, or compound solubility or dissolution. PBPK modeling significantly improved the DDI predictions of the 3D regimen with digoxin, where the predicted exposure ratios were within 1.25-fold of the clinical results (Table 4b). This improvement could be attributed to the fast absorption of digoxin ( $t_{max}$  ~1 hour) relative to the 3D regimen ( $t_{max}$  ~4 hours), and the low unbound concentrations of the 3D regimen.

For hepatic uptake transporters, only paritaprevir was predicted to inhibit OATPs (Table 4a). A minimal increase in the exposure of pravastatin and a moderate increase in the exposure of the rosuvastatin were observed (Menon et al., 2015); however; static R-values over-predicted the inhibition potential of the 3D regimen with OATP and BCRP substrates. Refinement of the DDI prediction using PBPK modeling suggested a significant improvement in DDI predictions with pravastatin and rosuvastatin within 2-fold of the clinical results (Table 4b). Unlike static models, PBPK modeling provides prediction for  $C_{max}$  ratios in addition to AUC, which is an important advantage in the case of transporters interactions at the intestinal and hepatic levels, where  $C_{max}$  may be significantly affected. Sensitivity analysis using the developed PBPK models revealed that interaction with pravastatin is mainly due to significant inhibition of hepatic

OATPs by paritaprevir, and interaction with rosuvastatin by inhibition of OATPs and BCRP by paritaprevir. This delineation of the main mechanism and perpetrator drug(s) that describes the observed interaction was possible because the Simcyp models of pravastatin and rosuvastatin explicitly described the contribution of each transporter mechanism, and the developed perpetrator models were also parameterized such that the in vitro IC<sub>50</sub> or K<sub>i</sub> for each transporter is entered separately and in each relevant organ (i.e. liver or gut). In fact the predicted AUCR for the 3D regimen with both statins were within 1.25-fold of observation, while predicted C<sub>max</sub> ratios were within 2-fold. Sensitivity analysis on paritaprevir BCRP IC<sub>50</sub> slightly improved the C<sub>max</sub> ratio predictions, suggesting that the rosuvastatin model in Simcyp is potentially missing an intestinal and or a hepatic transporter, which the 3D regimen inhibits. The PBPK approach improved accuracy of the DDI predictions to a satisfactory criterion within 1.25- to 2-fold of observed data reflecting the robustness of the PBPK modeling approach, and compared to the static basic and R-value models, a general conclusion regarding comparing the accuracy of these models cannot be drawn based on this small dataset alone. However, the PBPK approach may be considered as a translational tool for predicting transporter-based DDIs with the 3D regimen as perpetrators based on the prediction results in Table 4b, and for delineating the mechanisms of the complex interactions by the 3D regimen to allow for extrapolation to untested scenarios with concomitant medications. The presence of ritonavir within the 3D regimen may have complicated interpretation of the clinical DDI results; however, there are several clinical studies with ritonavir alone that may allow for delineating the observed DDI effects with the 3D regimen. For example, ritonavir alone did not alter the exposure of the OATP1B1 substrate pravastatin (Ieiri et al., 2013), while with the 3D regimen there was ~2-fold increase in pravastatin exposure, which was successfully predicted by PBPK simulations of the combined 3D regimen (Table 4b), and attributed to paritaprevir inhibition of OATP1B1.

Inhibition of renal transporters OAT1, OAT3, OCT2, MATE1 and MATE2K was also predicted to be clinically negligible. Consistent with these predictions, exposure of tenofovir (OAT1 substrate) and metformin (OCT2 substrate) did not change significantly following co-administration with the 3D regimen (Menon et al., 2014; Polepally et al., 2016).

Victim profile: Co-administration of strong CYP2C8 inhibitors or inducers with dasabuvir may cause significant changes in dasabuvir exposure, strong CYP3A inducers may cause significant decrease in systemic exposure of all drugs within the 3D regimen, while strong CYP3A4 inhibitors may cause a modest increase in paritaprevir and ritonavir systemic exposures, and minimal to no change to dasabuvir and ombitasvir exposures. The minimal inhibition of CYP3A is due to the presence of co-administered ritonavir, and compensating non-CYP mediated amide hydrolysis of ombitasvir (Shen et al., 2016b). It should be noted that in the presence of ritonavir within the 3D regimen where CYP3A metabolism of paritaprevir is nearly shut down, the high distribution of paritaprevir to the liver, is mainly driven by hepatic uptake transporters (OATP1B1/1B3). Thus, CYP inhibitors and probable inducers may only affect paritaprevir's systemic exposure but not liver exposure when used in combination with ritonavir, which is the target site of action.

Paritaprevir and M1 but not the other 3D components, are substrates for OATP1B1 and OATP1B3, while M1 is also a substrate of OCT1 (Table 1). These data are consistent with the observed increase in paritaprevir systemic exposure following co-administration with a mixed OATP/CYP3A inhibitor atazanavir (Khatri et al., 2016), Table 5. M1 systemic exposure was not affected by atazanavir, suggesting that it is a product of dasabuvir metabolism in liver rather than intestine, such that M1 is likely not available in portal blood at the liver inlet where inhibition of hepatic uptake transporters would be greatest. Alternatively, M1 may have other routes of elimination such as CYP3A hepatic metabolism (Table 1), and active hepatic uptake by OATPs may not be a rate limiting step for its disposition and elimination.

In addition, contribution of multiple transporters to paritaprevir disposition (Table 1) resulted in a modest increase in the systemic exposure of paritaprevir but not the other 3D components following co-administration with the mixed OATP, P-gp, BCRP and CYP3A4 inhibitor cyclosporine (Menon et al., 2015).

The minimal to modest increase in the systemic exposure of the 3D regimen following co-administration of a mixed CYP3A/P-gp inhibitor ketoconazole, suggests a possible contribution of P-gp to individual drugs within the 3D regimen. Contribution of BCRP was indirectly assessed clinically, where only the exposure of paritaprevir increased following co-administration with a single 30 mg dose of cyclosporine

(OATP, P-gp, BCRP and CYP3A4 inhibitor) (Menon et al., 2014) (Table 5), although this mixed interaction could be attributed to OATP inhibition alone. Thus for transporter-mediated victim DDIs, a qualitative assessment of the contribution of each transporter may be possible based on non-clinical and clinical studies with the 3D regimen, and a more mechanistic approach such as PBPK may be needed due to the complex interplay between metabolizing enzymes and transporters (Figure 1B).

Overall, for metabolism-mediated DDIs ritonavir predominates as a metabolism perpetrator (Figure 1A) leading to a net inhibition of CYP3A at the 100 mg boosting dose. For transporter-mediated DDIs paritaprevir and possibly ritonavir predominate as perpetrators leading to a net inhibition of OATPs, BCRP and a relatively mild or negligible inhibition of P-gp (Figure 1A). Drugs that are sensitive substrates of CYP3A, OATPs and BCRP and have a narrow therapeutic window are expected to have DDIs upon co-administration with the 3D regimen (Table 5). Victim profiles of the 3D regimen are depicted in Figure 1B, and semi-quantitative contributions of drug metabolizing enzymes are shown, while involvement of transporters is described qualitatively. Plasma exposures of the 3D regimen in combination with ritonavir were sensitive to strong CYP3A inducers but not significantly affected by strong CYP3A inhibitors, and only the plasma exposure of dasabuvir was sensitive to strong inhibitors of CYP2C8. Inhibitors of P-gp or BCRP increased plasma exposures of the 3D regimen, while plasma exposure of only paritaprevir was increased by OATP1B1/1B3 inhibitors (Table 5). It may be possible, in the future, to achieve a more quantitative extrapolation of the 3D regimen victim interactions with perpetrator drugs if PBPK models are constructed for each of the compounds in the 3D regimen.

In conclusion, this comprehensive metabolism and transporter assessment of the 3D regimen, and the model-based approach to predicting DDIs, may enable better clinical management of non-studied drug combinations with the 3D regimen.

## **Acknowledgments**

The authors would like to thank all members of the Drug Metabolism, Pharmacokinetics, and Bioanalysis department who contributed to studies and analyses that were used in this manuscript.

## **Authorship Contributions**

*Participated in research design:* Shebley, Liu, Bow

*Conducted experiments:* Shebley, Liu, Bow

*Performed data analysis:* Shebley, Liu, Bow

*Wrote or contributed to the writing of the manuscript:* Shebley, Liu, Kavetskaia, Sydor, de Morais, Fischer, Nijsen, Bow

## References

- AbbVie (2014) Viekira Pak, U.S. prescribing information.
- Badri P, Dutta S, Coakley E, Cohen D, Ding B, Podsadecki T, Bernstein B, Awni W and Menon R (2015) Pharmacokinetics and dose recommendations for cyclosporine and tacrolimus when coadministered with ABT-450, ombitasvir, and dasabuvir. *Am J Transplant* 15:1313-1322.
- Brown HS, Ito K, Galetin A and Houston JB (2005) Prediction of in vivo drug-drug interactions from in vitro data: impact of incorporating parallel pathways of drug elimination and inhibitor absorption rate constant. *Br J Clin Pharmacol* 60:508-518.
- Burger D, Back D, Buggisch P, Buti M, Craxi A, Foster G, Klinker H, Larrey D, Nikitin I, Pol S, Puoti M, Romero-Gomez M, Wedemeyer H and Zeuzem S (2013) Clinical management of drug-drug interactions in HCV therapy: challenges and solutions. *J Hepatol* 58:792-800.
- Chiou WJ, de Morais SM, Kikuchi R, Voorman RL, Li X and Bow DA (2014) In vitro OATP1B1 and OATP1B3 inhibition is associated with observations of benign clinical unconjugated hyperbilirubinemia. *Xenobiotica* 44:276-282.
- Fahmi OA, Hurst S, Plowchalk D, Cook J, Guo F, Youdim K, Dickins M, Phipps A, Darekar A, Hyland R and Obach RS (2009) Comparison of different algorithms for predicting clinical drug-drug interactions, based on the use of CYP3A4 in vitro data: predictions of compounds as precipitants of interaction. *Drug Metab Dispos* 37:1658-1666.
- Fahrmayr C, Fromm MF and Konig J (2010) Hepatic OATP and OCT uptake transporters: their role for drug-drug interactions and pharmacogenetic aspects. *Drug Metab Rev* 42:380-401.
- FDA US (2012) Drug Interaction Studies — Study Design, Data Analysis, Implications for Dosing, and Labeling Recommendations.
- Feld JJ, Kowdley KV, Coakley E, Sigal S, Nelson DR, Crawford D, Weiland O, Aguilar H, Xiong J, Pilot-Matias T, DaSilva-Tillmann B, Larsen L, Podsadecki T and Bernstein B (2014) Treatment of HCV with ABT-450/r-ombitasvir and dasabuvir with ribavirin. *N Engl J Med* 370:1594–1603.
- Gartzke D and Fricker G (2014) Establishment of optimized MDCK cell lines for reliable efflux transport studies. *J Pharm Sci* 103:1298-1304.



- Ieiri I, Tsunemitsu S, Maeda K, Ando Y, Izumi N, Kimura M, Yamane N, Okuzono T, Morishita M, Kotani N, Kanda E, Deguchi M, Matsuguma K, Matsuki S, Hirota T, Irie S, Kusuhara H, Sugiyama Y (2013) Mechanisms of pharmacokinetic enhancement between ritonavir and saquinavir; micro/small dosing tests using midazolam (CYP3A4), fexofenadine (p-glycoprotein), and pravastatin (OATP1B1) as probe drugs. *J Clin Pharmacol* 53: 654-661
- Jamei M, Bajot F, Neuhoff S, Barter Z, Yang J, Rostami-Hodjegan A and Rowland-Yeo K (2014) A mechanistic framework for in vitro-in vivo extrapolation of liver membrane transporters: prediction of drug-drug interaction between rosuvastatin and cyclosporine. *Clin Pharmacokinet* 53:73-87.
- Khalilieh S, Feng HP, Hulskotte EG, Wenning LA and Butterton JR (2015) Clinical pharmacology profile of boceprevir, a hepatitis C virus NS3 protease inhibitor: focus on drug-drug interactions. *Clin Pharmacokinet* 54:599-614.
- Khatri A, Dutta S, Wang H, Podsadecki T, Trinh R, Awni W and Menon R (2016) Evaluation of drug-drug interactions between hepatitis C antiviral agents ombitasvir, paritaprevir/ritonavir, and dasabuvir and HIV-1 protease inhibitors. *Clin Infect Dis* 62:972-979.
- Kikuchi R, Lao Y, Bow DA, Chiou WJ, Andracki ME, Carr RA, Voorman RL and De Morais SM (2013) Prediction of clinical drug-drug interactions of veliparib (ABT-888) with human renal transporters (OAT1, OAT3, OCT2, MATE1, and MATE2K). *J Pharm Sci* 102:4426-4432.
- Kirby BJ, Symonds WT, Kearney BP and Mathias AA (2015) Pharmacokinetic, Pharmacodynamic, and Drug-Interaction Profile of the Hepatitis C Virus NS5B Polymerase Inhibitor Sofosbuvir. *Clin Pharmacokinet* 54:677-690.
- Kumar GN, Rodrigues AD, Buko AM and Denissen JF (1996) Cytochrome P450-mediated metabolism of the HIV-1 protease inhibitor ritonavir (ABT-538) in human liver microsomes. *J Pharmacol Exp Ther* 277:423-431.
- Maasoumy B, Port K, Calle Serrano B, Markova AA, Sollik L, Manns MP, Cornberg M and Wedemeyer H (2013) The clinical significance of drug-drug interactions in the era of direct-acting anti-viral agents against chronic hepatitis C. *Aliment Pharmacol Ther* 38:1365-1372.

- Menon R, Badri P, Khatri A, Wang T, Bow DA, Polepally A, Podsadecki T, Awni WM and Dutta S (2014) ABT-450/Ritonavir +Ombitasvir + Dasabuvir: Drug Interactions Mediated by Transporters in *15th International Workshop on Clinical Pharmacology of HIV and Hepatitis Therapy*, Washington, DC.
- Menon RM, Badri PS, Wang T, Polepally AR, Zha J, Khatri A, Wang H, Hu B, Coakley EP, Podsadecki TJ, Awni WM and Dutta S (2015) Drug-drug interaction profile of the all-oral anti-hepatitis C virus regimen of paritaprevir/ritonavir, ombitasvir, and dasabuvir. *J Hepatol* 63:20-29.
- Menon RM, Klein CE, Podsadecki TJ, Chiu YL, Dutta S and Awni WM (2016) Pharmacokinetics and tolerability of paritaprevir, a direct acting antiviral agent for hepatitis C virus treatment, with and without ritonavir in healthy volunteers. *Br J Clin Pharmacol* 81:929-940.
- Mensing S, Polepally AR, Konig D, Khatri A, Liu W, Podsadecki TJ, Awni WM, Menon RM and Dutta S (2016) Population pharmacokinetics of paritaprevir, ombitasvir, dasabuvir, ritonavir, and ribavirin in patients with hepatitis C virus genotype 1 infection: combined analysis from 9 phase 1b/2 studies. *AAPS J* 18:270-280.
- Neuhoff S, Yeo KR, Barter Z, Jamei M, Turner DB and Rostami-Hodjegan A (2013) Application of permeability-limited physiologically-based pharmacokinetic models: part II - prediction of P-glycoprotein mediated drug-drug interactions with digoxin. *J Pharm Sci* 102:3161-3173.
- Polepally AR, King JR, Ding B, Shuster DL, Dumas EO, Khatri A, Chiu YL, Podsadecki TJ and Menon RM (2016) Drug-drug interactions between the anti-hepatitis C virus 3D regimen of ombitasvir, paritaprevir/ritonavir, and dasabuvir and eight commonly used medications in healthy volunteers. *Clin Pharmacokinet* 55:1003-1014.
- Rowland Yeo K, Jamei M, Yang J, Tucker GT and Rostami-Hodjegan A (2010) Physiologically based mechanistic modelling to predict complex drug-drug interactions involving simultaneous competitive and time-dependent enzyme inhibition by parent compound and its metabolite in both liver and gut - the effect of diltiazem on the time-course of exposure to triazolam. *Eur J Pharm Sci* 39:298-309.
- Shen J, Serby M, Reed A, Lee AJ, Menon R, Zhang X, Marsh K, Wan X, Kavetskaia O and Fischer V (2016a) Metabolism and Disposition of Hepatitis C Polymerase Inhibitor Dasabuvir in Humans. *Drug Metab Dispos* 44:1139-1147.

- Shen J, Serby M, Surber B, Lee AJ, Ma J, Badri P, Menon R, Kavetskaia O, de Morais SM, Sydor J and Fischer V (2016b) Metabolism and disposition of pan-genotypic inhibitor of hepatitis C virus NS5A ombitasvir in humans. *Drug Metab Dispos* 44:1148-1157.
- Soriano V, Labarga P, Barreiro P, Fernandez-Montero JV, de Mendoza C, Esposito I, Benitez-Gutierrez L and Pena JM (2015) Drug interactions with new hepatitis C oral drugs. *Expert Opin Drug Metab Toxicol* 11:333-341.
- Varma MV, Lai Y, Feng B, Litchfield J, Goosen TC and Bergman A (2012) Physiologically based modeling of pravastatin transporter-mediated hepatobiliary disposition and drug-drug interactions. *Pharm Res* 29:2860-2873.
- WHO (2011) Hepatitis C. *Wkly Epidemiol Rec* 86:445-447.
- Yeh RF, Gaver VE, Patterson KB, Rezk NL, Baxter-Meheux F, Blake MJ, Eron JJ, Jr., Klein CE, Rublein JC and Kashuba AD (2006) Lopinavir/ritonavir induces the hepatic activity of cytochrome P450 enzymes CYP2C9, CYP2C19, and CYP1A2 but inhibits the hepatic and intestinal activity of CYP3A as measured by a phenotyping drug cocktail in healthy volunteers. *J Acquir Immune Defic Syndr* 42:52-60.
- Zhou J, Tracy TS and Remmel RP (2011) Correlation between bilirubin glucuronidation and estradiol-3-glucuronidation in the presence of model UDP-glucuronosyltransferase 1A1 substrates/inhibitors. *Drug Metab Dispos* 39:322-329.
- Shi JG, Zhang Y and Yeleswaram S (2011) The relevance of assessment of intestinal P-gp inhibition using digoxin as an in vivo probe substrate. *Nature Rev Drug Discovery* 10:75
- Nader AM and Foster DR (2013) Suitability of Digoxin as a P-Glycoprotein Probe: Implications of Other Transporters on Sensitivity and Specificity. *J Clin Pharm* 54:3-13




## Footnotes

The studies in this manuscript were sponsored by AbbVie; M.S., D.A.J.B., J.L., O.K., S.M.D.M., V.F., J.S., and M.J.M.A.N. are employees of AbbVie. M.S. and D.A.J.B. have contributed equally to writing this manuscript.

Please send reprint requests to: Mohamad Shebley, Department of Clinical Pharmacology and Pharmacometrics, AbbVie Inc., 1. N. Waukegan Road, Bldg. AP31, 3<sup>rd</sup> floor, North Chicago, IL, 60064; tel: (847)938-3662; fax: (847)938-5193; email: [mohamad.shebley@abbvie.com](mailto:mohamad.shebley@abbvie.com)

**Figure legends:**

**Figure 1.** Schematic representation of drug metabolizing enzymes and drug transporters demonstrated to be affected by the 3D regimen as perpetrators (A) and important pathways involved in the disposition and elimination of the 3D regimen as victims (B).

In Figure 1A,  represents strong inhibition of an enzyme/transporter;  represents induction of an enzyme/transporter;  represents weak inhibition of an enzyme or transporter. Ritonavir is responsible for intestinal and hepatic CYP3A4 net inhibition and DDI with co-administered substrates, and moderate induction of CYP2C19; paritaprevir is responsible for inhibition of OATP1B1, OATP1B3 and BCRP and resulting DDI with co-administered substrates; 3D regimen inhibit UGT1A1 and results in weak or moderate but not clinically relevant DDI with co-administered substrates (i.e. raltegravir)

In Figure 1B, intensity of arrows represents degree of pathway contribution to disposition and elimination of 3D regimen, where thick arrows represent high contribution and vice versa. For simplicity, arrows are only shown in a hepatocyte in this schematic. Dashed arrows indicate qualitative contribution of a corresponding mechanism. For CYP3A4 metabolism of drugs within 3D regimen, co-administered ritonavir mostly diminishes the contribution of this pathway (see results and discussion for more detail).

Figure abbreviations: P-gp: P-glycoprotein; BCRP: Breast Cancer Resistance Protein; OATP: organic anion transport polypeptide; PTV: paritaprevir; RTV: ritonavir; DSV: dasabuvir; M1: metabolite of dasabuvir; OBV: ombitasvir.

**Tables**

**Table 1.** *In vitro* enzyme and transporters victim data summary of paritaprevir, ritonavir, ombitasvir, dasabuvir, and M1

Enzyme or Transporter (endpoint or unit)	Paritaprevir	Ritonavir	Ombitasvir	Dasabuvir	M1
CYP2C8 (% contribution)	-	-	-	~60	<10
CYP3A4 (%contribution) <sup>a</sup>	~100, <50 with ritonavir	~100, <50 due to auto-inhibition	~100, <10 with ritonavir	~30, <10 with ritonavir	~100, <10 with ritonavir
P-gp/MDR-1 (net efflux ratio <sup>b</sup> )	13	26	44	6	32
BCRP (net efflux ratio)	5	-	-	2	2
OATP1B1 (Km <sup>c</sup> , μM)	0.2	-	-	-	1.3
OATP1B3 (Km, μM)	0.1	-	-	-	1.7
OCT1	-	-	-	-	substrate

CYP contribution results are from incubations with individual recombinant human isoforms, dasabuvir based on chemical inhibition in human liver microsomes; ritonavir based on correlation analysis in human liver microsomes.

<sup>a</sup> CYP3A4 contribution shown as individual drug *in vitro* results first followed by overall contribution within 3D regimen where ritonavir is co-administered

<sup>b</sup> ER = efflux ratio from MDCKII cells over expressing P-gp or BCRP (normalized for efflux in wild-type MDCKII cells).

<sup>c</sup> Michaelis-Menton kinetics constant (Km) was generated following initial active uptake screening studies (see Materials and Methods).

( - ) Not a substrate based on *in vitro* studies.

**Table 2.** Parameters used in predictions of 3D regimen as perpetrators of enzyme and transporter inhibition using basic and mechanistic static models

Drug	M.W.	Dose (mg)	$f_{u,p}$ <sup>a</sup>	$f_{u,b}$ <sup>b</sup>	$C_{max,ss}$ or $[I]_1$ (ng/mL)	$[I]_h$ <sup>c</sup> (ng/mL)	$[I]_2$ <sup>d</sup> (ng/mL)	Fa or Fa*Fg	Ka <sup>e</sup> (hr <sup>-1</sup> )
Paritaprevir	765.89	150	0.020	0.029	1470	54.6	600	1	0.25
Ritonavir	720.96	100	0.011	0.018	1600	32.5	100	1	0.17
Ombitasvir	894.12	25	0.0003	0.0003	127	0.1	400	1	0.21
Dasabuvir	493.58	250	0.004	0.006	1030	14.8	1000	1	0.58
M1	509.58	--	0.066	0.094	660	--	--	--	--

M.W. is molecular weight (g/mole).

<sup>a</sup> Generally  $f_{u,p}$  determined from *in vitro* studies where tested concentration of each drug is near its  $C_{max,ss}$ .

<sup>b</sup>  $f_{u,b}$  is calculated from  $f_{u,p}$  and the blood to plasma ratio.

<sup>c</sup> Hepatic inlet concentration as described in equation 1 in Materials and Methods.

<sup>d</sup>  $[I]_2$  is oral dose amount of inhibitor/250 mL as described in equation 2 in Materials and Methods.

<sup>e</sup> Ka is estimated from clinical population pharmacokinetics analysis (Mensing et al., 2016).

Fa and Fg are fractions of the dose of inhibitor which is absorbed and escape gut metabolism/extraction, respectively.

(--) Parameters were not calculated for the metabolite since it was not dosed orally.

**Table 3.** Calculated model parameters and predicted AUCR values for 3D regimen based on mechanistic static model or basic model for reversible CYP/UGT inhibition for individual components or combined regimen

Enzyme	Paritaprevir	Ritonavir	Ombitasvir	Dasabuvir	M1	3D Regimen		
	AUCR <sub>(pred)</sub>	AUCR <sub>(pred)</sub>	AUCR <sub>(pred)</sub>	AUCR <sub>(pred)</sub>	R <sub>1(pred)</sub>	cAUCR <sub>(pred)</sub>	cAUCR <sub>(obs)</sub>	Pred/Obs
CYP2C9	--	1.17	--	1.01	--	1.17	0.9 <sup>a</sup>	1.3
CYP2C19	--	1.02	--	1.00	--	1.02	0.6 <sup>a</sup>	1.7
CYP3A4	--	28.2	--	--	--	28.2	57 <sup>b</sup>	0.5
UGT1A1	1.04	1.05	1.00	1.06	1.03	1.20	2.4 <sup>c</sup>	0.5

NT = not tested; (--) parameters were not calculated because IC<sub>50</sub> could not be estimated due to no or low inhibition at the highest tested concentration *in vitro*

AUCR<sub>(pred)</sub> calculations for the reversible CYP inhibition using the mechanistic static model as described in equation 1 (Materials and Methods)

R<sub>1(pred)</sub> calculation from a modified basic model for predicting reversible CYP inhibition;  $R_1 = 1 + [I]/K_i$  where [I] is unbound C<sub>max</sub> of inhibitor, and K<sub>i</sub> (or IC<sub>50</sub>/2) is *in vitro* inhibition constant; M1 is a metabolite of dasabuvir, thus R<sub>1</sub> model was used for DDI predictions

cAUCR; combination AUCR prediction as described in Materials and Methods

<sup>a</sup> (Menon et al., 2015)

<sup>b</sup> (Badri et al., 2015)

<sup>c</sup> (Khatri et al., 2016)



**Table 4a.** Calculated model parameters and predictions of 3D regimen as perpetrators of intestinal or systemic efflux transporters, and hepatic uptake transporters

Drug	Intestinal/Hepatic/Renal				Hepatic		
	P-gp		BCRP		OATP1B1	OATP1B3	OCT1
	[I <sub>2</sub> ]/IC <sub>50</sub>	[I <sub>1</sub> ]/IC <sub>50</sub>	[I <sub>2</sub> ]/IC <sub>50</sub>	[I <sub>1</sub> ]/IC <sub>50</sub>	R-value <sup>a</sup>		
Paritaprevir	20.6	0.05	1328	3.25	2.6	3.9	--
Ritonavir	1585	6.34	23.1	0.09	1.05	1.05	1.01
Ombitasvir	--	--	--	--	--	--	--
Dasabuvir	121	0.12	130	0.13	1.02	1.00	--
M1	--	0.02	--	0.02	1.03	1.01	--

[I]<sub>1</sub> represents the mean steady-state total (free and bound) C<sub>max</sub> following administration of the highest proposed clinical dose as described in equation 3 in Materials and Methods.

[I]<sub>2</sub> is oral dose of inhibitor/250 mL as described in equation 4 in Materials and Methods.

<sup>a</sup>R-value is ratio of unbound inhibitor concentration at the inlet to liver to *in vitro* IC<sub>50</sub>, as described in equation 5 in Materials and Methods.

(--) parameters were not calculated because IC<sub>50</sub> could not be estimated due to no or low inhibition at the highest tested concentration *in vitro*

**Table 4b.** PBPK model predictions of 3D regimen as perpetrators of intestinal and hepatic efflux and hepatic uptake transporters compared to clinical results

Victim Drug (exposure ratios with inhibitors)	Digoxin (P-gp)		Rosuvastatin (BCRP + OATP1B1/1B3)		Pravastatin (OATP1B1/1B3)	
	Predicted	Observed <sup>a</sup>	Predicted	Observed <sup>a</sup>	Predicted	Observed <sup>a</sup>
C <sub>max</sub> ratio	1.19	1.15	3.42, 4.10 <sup>b</sup>	7.13	2.0	1.37
AUC ratio	1.20	1.16	2.41, 2.55 <sup>b</sup>	2.59	2.16	1.82

<sup>a</sup> (Menon et al., 2015)

<sup>b</sup> Results from sensitivity analysis simulations on paritaprevir and ritonavir *in vitro* IC<sub>50</sub> values against intestinal BCRP.

**Table 5.** Summary of important mechanism-based DDI predictions and clinical observations of the 3D regimen

Mechanism	Perpetrator		Victim	
	DDI predictions	Clinical observations	DDI predictions	Clinical observations
CYP3A	Ritonavir ↑ Sensitive substrates	Ritonavir ↑ Paritaprevir & Tacrolimus	↓ 3D regimen with strong inducers ↔ 3D regimen with strong inhibitors	↓ 3D regimen with Carbamazepine ↔ 3D regimen with Ketoconazole
CYP2C8	None	--	↑ Dasabuvir with strong inhibitors	↑ Dasabuvir with Gemfibrozil
CYP2C19	Ritonavir & Dasabuvir ↔ Sensitive substrates <sup>b</sup>	Ritonavir ↓ Omeprazole <sup>a</sup>	None	--
OATP1B1 & OATP1B3	Paritaprevir ↑ Sensitive substrates	Paritaprevir ↑ Pravastatin	↑ Paritaprevir with strong inhibitors	↑ Paritaprevir <sup>a</sup> with Atazanavir
BCRP	Paritaprevir ↑ Sensitive substrates	Paritaprevir ↑ Rosuvastatin	↑ 3D regimen with strong inhibitors	↑ 3D regimen <sup>a</sup> with Cyclosporine
UGT1A1	3D regimen ↑ Sensitive substrates	3D regimen ↑ Raltegravir <sup>a</sup>	None	--

↑ or ↓ or ↔ = increase or decrease or no change in systemic exposure, respectively.

(--) mechanism was not tested in dedicated clinical trials.

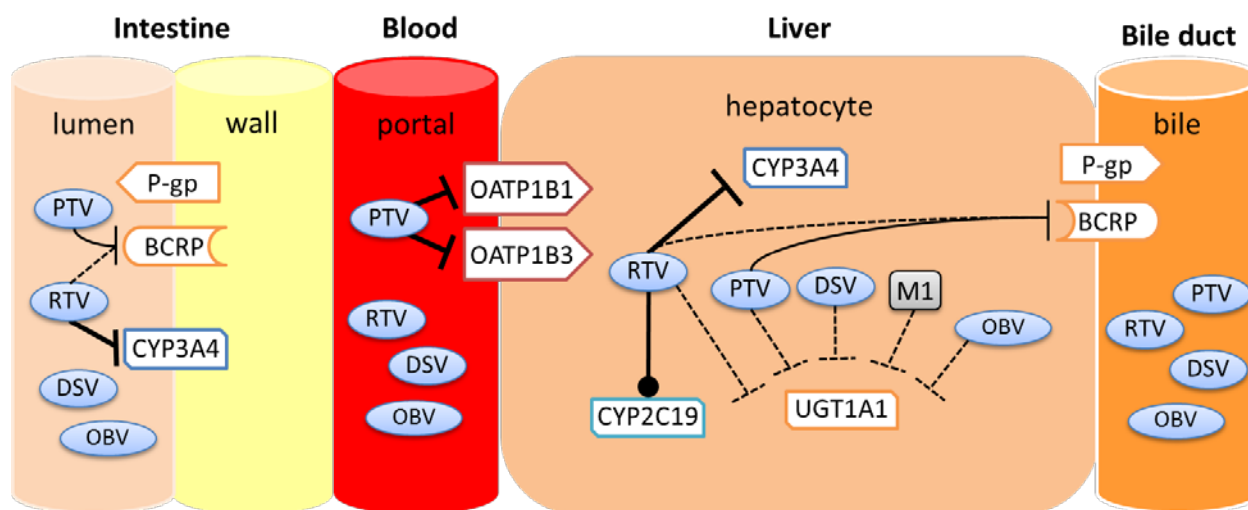
<sup>a</sup> Change in exposure is not clinically relevant (Badri et al., 2015; Khatri et al., 2016).

<sup>b</sup> CYP2C19 induction was not considered in DDI predictions due to unavailability of model parameters EC<sub>50</sub> & E<sub>max</sub> for ritonavir.

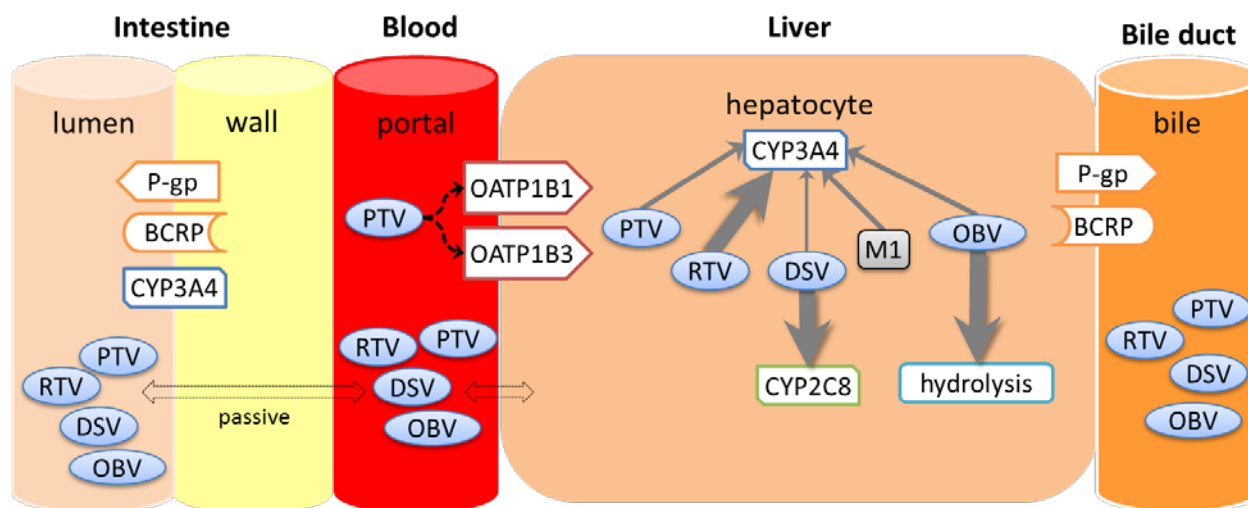
Additional information: carbamazepine (strong CYP3A inducer), ketoconazole (strong CYP3A inhibitor), gemfibrozil (strong CYP2C8 inhibitor), atazanavir (OATP & CYP3A inhibitor), cyclosporine (OATP, P-gp and BRP inhibitor), pravastatin (OATP1B1 and OATP1B3 substrate), rosuvastatin (OATP and BCRP substrate), raltegravir (UGT1A1 substrate).

**Figure 1.** Schematic representation of drug metabolizing enzymes and drug transporters demonstrated to be affected by the 3D regimen as perpetrators (A) and important pathways involved in the disposition and elimination of the 3D regimen as victims (B).

(A)



(B)



**Supplemental Data to:*****Drug Metabolism and Disposition*****Mechanisms and Predictions of Drug-Drug Interactions of the Hepatitis C Virus 3-Direct Acting Antiviral (3D) Regimen: Paritaprevir/Ritonavir, Ombitasvir and Dasabuvir**

Mohamad Shebley, Jinrong Liu, Olga Kavetskaia, Jens Sydor, Sonia M. de Morais, Volker Fischer,  
Marjoleen J.M.A. Nijsen, Daniel A.J. Bow

Drug Metabolism, Pharmacokinetics and Bioanalysis (M.S., J.L., O.K., J.S., S.M.D.M., V.F., M.J.M.A.N.,  
D.A.J.B.), Clinical Pharmacology and Pharmacometrics (M.S.), AbbVie Inc., North Chicago, Illinois

**Supplemental Table 1. CYP inhibition assay conditions.**

CYP	Substrate	Metabolite	Inhibitor	Substrate	HLM	Incubation
				Concentration	protein	
				( $\mu$ M)	(mg/mL)	(min)
CYP1A2	Phenacetin	Acetaminophen	Furafylline	25	0.1	30
CYP2B6	Bupropion	Hydroxy bupropion	Ticlopidine	75	0.05	10
CYP2C8	Paclitaxel	6 $\alpha$ -hydroxytaxol	Quercetin	10	0.4	15
CYP2C9	Diclofenac	4-hydroxy diclofenac	Sulfaphenazole	5	0.05	10
CYP2C19	S-Mephenytoin	4'-hydroxy mephenytoin	Tranylcypromine	22	0.2	40
CYP2D6	Dextromethorphan	Dextrorphan	Quinidine	2.5	0.05	30
CYP3A4	Midazolam	1-hydroxy midazolam	Troleandomycin	4	0.05	10
CYP3A4	Testosterone	6 $\beta$ -hydroxy testosterone	Ketoconazole	50	0.05	10

**Supplemental Table 2. UGT inhibition assay conditions.**

<b>UGT</b>	<b>Substrate</b>	<b>Inhibitor</b>	<b>Substrate Concentration (<math>\mu</math>M)</b>	<b>HLM Protein (mg/mL)</b>	<b>Incubation (min)</b>
UGT1A1	$\beta$ -estradiol	Chrysin	10	0.025	20
UGT1A4	Trifluoperazine HCl	Efavirenz	40	0.020	20
UGT1A6	5-Hydroxytryptophol	1-Naphthol	250	0.020	20
UGT1A9	Propofol	Niflumic Acid	50	0.020	20
UGT2B7	Zidovudine	Mefenamic Acid	500	0.020	50

**Supplemental Table 3. CYP time-dependent inhibition assay conditions.**

CYP	Substrate	Metabolite	Substrate		Inhibitor	
			Conc ( $\mu$ M)	Positive Control (Inhibitor)	Conc. ( $\mu$ M)	Pre-Incubation Time (min)
CYP3A4	midazolam	1'-hydroxy midazolam	40	Troleandomycin	10, 50	0, 30
CYP3A4	testosterone	6 $\beta$ -hydroxy testosterone	300	Troleandomycin	1, 10	0, 30
CYP1A2	phenacetin	acetaminophen	250	Furafylline	1, 10	0, 20
CYP2B6	bupropion	Hydroxy bupropion	400	Ticlopidine	1, 10	0, 30
CYP2C8	paclitaxel	6-hydroxy paclitaxel	50	Phenelzine	50, 250	0, 20
CYP2C9	diclofenac	4-hydroxy diclofenac	50	Tienilic Acid	1, 10	0, 10
CYP2C19	S-mephenytoin	4-hydroxy mephenytoin	250	Ticlopidine	1, 10	0, 15
CYP2D6	dextromethorphan	dextrorphan	50	Paroxetine	1, 10	0, 30

**Supplemental Table 4. CYP probe sets used in induction studies.**

<b>CYP</b>	<b>Probe</b>
	Forward: 5'- CTT CAT CCA ATG GAC TGC ATA AAT- 3'
CYP3A4	Reverse: 5'- TCC CAA GTA TAA CAC TCT ACA CAG ACA A- 3'
	TaqMan: 5'-/56FAM/CCG GGG ATT CTG TAC ATG CAT TG/3BHQ_1/- 3'
CYP2B6	TaqMan® Gene Expression Assay: Invitrogen Cat. 4331182 Assay ID: Hs03044634_m1.
	Forward: 5'- TGG CTT CTA CAT CCC CAA GAA A- 3'
CYP1A2	Reverse: 5'- CCA CAG CTC TGG GTC ATG GT- 3'
	TaqMan: 5'-/56FAM/CTG CCA CTG GTT TAC GAA GAC ACA /3BHQ_1/- 3'
	Forward: 5'-TTC ACC AAG CGT TGG ATT GTT -3'
28S	Reverse: 5'-TGT CTG AAC CTG CGG TTC CT -3'
	TaqMan: 5'-/56FAM/TCA CGA CGG TCT AAA CCC AGC TCA CG/3BHQ_1/- 3'5



**Supplemental Table 5: Paritaprevir PBPK model input parameters in Simcyp V14.1**

<b>Paritaprevir</b>	<b>Value/Assumption</b>	<b>Source</b>
<b>PhysChem and Blood Binding</b>		
Mol Weight (g/mol)	765.88	Product label
log P	3.1	Internal data
Compound Type	Monoprotic Base	
pKa 1	4.6	
B/P	0.7	Product label
fu	0.02	
<b>Absorption</b>		
Absorption Model	1st order	
fa	1	Estimated from oral PK
ka (1/h)	0.25	
fu(Gut)	1	Assumed
Q(Gut) L/hr	5.7	Predicted
<b>Distribution</b>		
Distribution Model	Minimal PBPK	
SAC Q (L/h)	1.0	Estimated from intravenous PK
Volume [Vsac] (L/kg)	0.1	
Vss (L/kg)	1.0	
Liver Kp	40	
<b>Elimination</b>		
Clearance Type	In Vivo Clearance	
CL (po) (L/h)	20	Observed from oral PK
Active Uptake into Hepatocyte	4	Estimated from DDI data
<b>Transporters Interaction</b>		
Organ/Tissue	Gut	In vitro
ABCB1 (P-gp) $K_{i,u}^{\#}$ ( $\mu$ M)	38.1	
ABCG2 (BCRP) $K_{i,u}^{\#}$ ( $\mu$ M)	0.6	
ABCC2 (MRP2) $K_{i,u}^{\#}$ ( $\mu$ M)	12	
Organ/Tissue	Liver	
ABCB1 (P-gp) $K_{i,u}^{\#}$ ( $\mu$ M)	38.1	
ABCC2 (MRP2) $K_{i,u}^{\#}$ ( $\mu$ M)	12	
SLCO1B1 (OATP1B1) $K_{i,u}^{\#}$ ( $\mu$ M)	0.031	
SLCO1B3 (OATP1B3) $K_{i,u}^{\#}$ ( $\mu$ M)	0.017	
ABCG2 (BCRP) $K_{i,u}^{\#}$ ( $\mu$ M)	0.60	

<sup>#</sup>  $K_{i,u}$  =  $IC_{50}$  from *in vitro* experiments

Supplemental Table 6: Ritonavir PBPK model input parameters in Simcyp V14.1

Ritonavir	Value/Assumption	Source
<b>PhysChem and Blood Binding</b>		
Mol Weight (g/mol)	720.95	Product label
log P	4.3	Internal data
Compound Type	Diprotic Base	
pKa 1	2.8	
pKa 2	2.8	
B/P	0.6	
fu	0.006	
<b>Absorption</b>		
Absorption Model	1st order	
fa	1	Estimated from oral PK
ka (1/h)	0.4	
lag time (h)	1.5	
fu(Gut)	1.0	Assumed
<b>Distribution</b>		
Distribution Model	Minimal PBPK	
SAC Q (L/h)	0.65	Estimated from oral PK
Volume [V <sub>sac</sub> ] (L/kg)	0.1	
V <sub>ss</sub> (L/kg)	0.38	
<b>Elimination</b>		
Clearance Type	In Vivo Clearance	
CL (po) (L/h)	11	Observed from oral PK
<b>CYPs and/or UGTs Interaction</b>		
CYP3A4 K <sub>i,u</sub> (μM)	0.0003	Optimized based on in vitro and clinical published data
CYP3A4 MBI K <sub>app,u</sub> (μM)	0.0005	
CYP3A4 MBI K <sub>inact</sub> (1/h)	0.04	
CYP3A4 Ind max	12.7	
CYP3A4 Ind C <sub>50,u</sub> (μM)	2.4	
<b>Transporters Interaction</b>		
Organ/Tissue	Gut	In vitro
ABCB1 (P-gp) K <sub>i,u</sub> <sup>#</sup> (μM)	0.35	
ABCG2 (BCRP) K <sub>i,u</sub> <sup>#</sup> (μM)	24	
Organ/Tissue	Liver	
SLCO1B1 (OATP1B1) K <sub>i,u</sub> <sup>#</sup> (μM)	0.5	
SLCO1B3 (OATP1B3) K <sub>i,u</sub> <sup>#</sup> (μM)	0.6	
ABCB1 (P-gp) K <sub>i,u</sub> <sup>#</sup> (μM)	0.35	
ABCG2 (BCRP) K <sub>i,u</sub> <sup>#</sup> (μM)	24	

<sup>#</sup> K<sub>i,u</sub> = IC<sub>50</sub> from *in vitro* experiments

Supplemental Table 7: Dasabuvir PBPK model input parameters in Simcyp V14.1

Dasabuvir	Value/Assumption	Source
<b>PhysChem and Blood Binding</b>		
Mol Weight (g/mol)	493.57	Product label
log P	4.37	Internal data
Compound Type	Diprotic Acid	
pKa 1	8.2	
pKa 2	9.2	
B/P	0.7	
fu	0.0041	
<b>Absorption</b>		
Absorption Model	1st order	Estimated from oral PK
fa	0.8	
ka (1/h)	0.5	
lag time (h)	2	
fu(Gut)	0.0041	Assumed
<b>Distribution</b>		
Distribution Model	Minimal PBPK	Estimated from intravenous PK
SAC Q (L/h)	40	
Volume [Vsac] (L/kg)	1.5	
Vss (L/kg)	2.07	
<b>Elimination</b>		
Clearance Type	In Vivo Clearance	Observed from oral PK
CL (po) (L/h)	33	
<b>Transporters Interaction</b>		
Organ/Tissue	Gut	In vitro
ABCB1 (P-gp) $K_{i,u}^{\#}$ ( $\mu\text{M}$ )	16.7	
ABCG2 (BCRP) $K_{i,u}^{\#}$ ( $\mu\text{M}$ )	15.6	
ABCC2 (MRP2) $K_{i,u}^{\#}$ ( $\mu\text{M}$ )	52	
Organ/Tissue	Liver	
SLCO1B1 (OATP1B1) $K_{i,u}^{\#}$ ( $\mu\text{M}$ )	0.9	
SLCO1B3 (OATP1B3) $K_{i,u}^{\#}$ ( $\mu\text{M}$ )	6.6	
ABCB1 (P-gp) $K_{i,u}^{\#}$ ( $\mu\text{M}$ )	16.7	
ABCC2 (MRP2) $K_{i,u}^{\#}$ ( $\mu\text{M}$ )	52	
ABCG2 (BCRP) $K_{i,u}^{\#}$ ( $\mu\text{M}$ )	15.6	

<sup>#</sup>  $K_{i,u} = IC_{50}$  from *in vitro* experiments

**Supplemental Table 8. *In vitro* CYP, UGT, and transporters inhibition potency of paritaprevir, ritonavir, ombitasvir, dasabuvir, and M1**

Enzyme or Transporter	IC <sub>50</sub> (μM)				
	Paritaprevir	Ritonavir	Ombitasvir	Dasabuvir	M1
CYP2B6	-	1.0	-	29	-
CYP2C8	13	1.52	7.4	16.5	-
CYP2C9	-	0.57	-	8.6	-
CYP2C19	-	4.28	-	17.5	-
CYP2D6	-	1.04	-	42.5	-
CYP3A4	-	0.006 <sup>a</sup> 0.03 <sup>b</sup>	-	-	-
UGT1A1	3.6	1.7 <sup>c</sup>	2.1	0.92	5.1
UGT1A4	6.8	NT	-	3.8	10.2
UGT1A6	46.7	NT	-	3.4	-
UGT1A9	-	NT	-	6.5	46.6
UGT2B7	-	NT	-	41.9	-
P-gp	38.1	0.35	-	16.7	80.6
BCRP	0.59	24	-	15.6	54.7
MRP2	12	-	-	52	22
OATP1B1	0.03	0.5	-	0.9	2.6
OATP1B3	0.02	0.6	-	6.6	9.7
OCT1	-	2.5	-	-	-
OAT1	14	14	-	-	-
OAT3	95	8.1	-	-	-
MATE1	-	3.3	-	-	28
MATE2K	170	90	-	-	72

<sup>a</sup> Using midazolam as a probe substrate; <sup>b</sup> using testosterone as a probe substrate; (-) IC<sub>50</sub> could not be estimated due to no or low inhibition at the highest tested concentration *in vitro*; NT = not tested.

Additional information: CYP and UGT IC<sub>50</sub> values were generated from human liver microsomes incubations at optimized conditions (see Materials and Methods); transporters IC<sub>50</sub> values were generated from cell lines overexpressing specific transporter or membrane vesicles expressing specific transporter (see Materials and Methods).

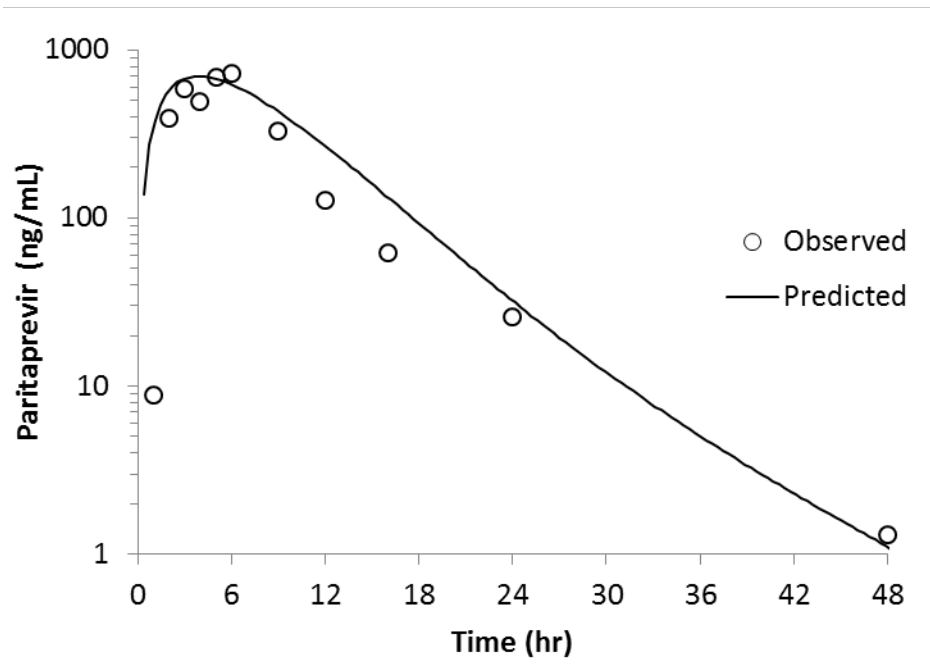
<sup>c</sup> (Zhou et al., 2011)

**Supplemental Table 9. *In vitro* CYP induction by paritaprevir, ritonavir, ombitasvir, dasabuvir, and M1**

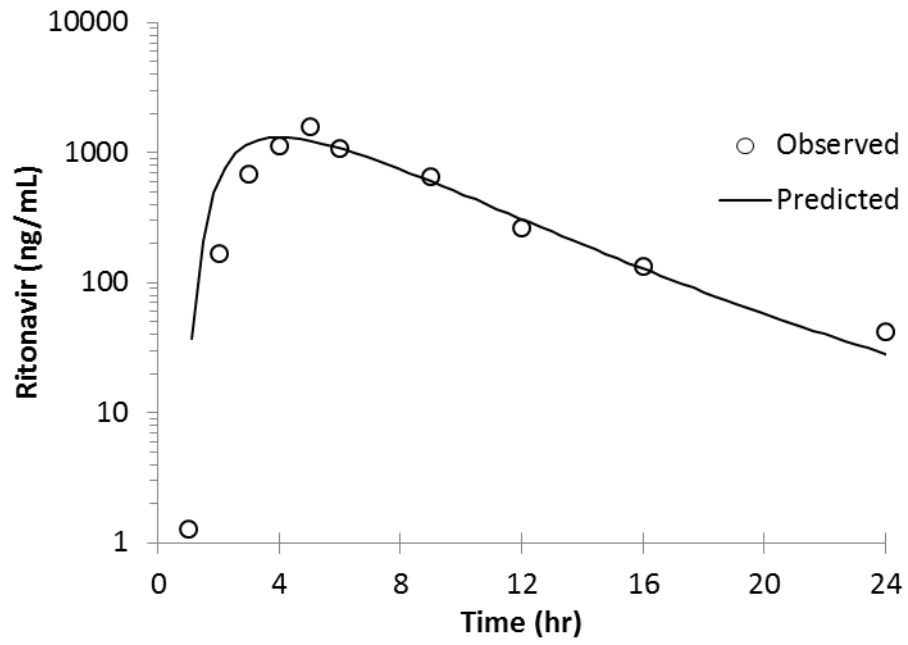
Enzyme	CYP mRNA induction (fold over vehicle / % of positive control <sup>*</sup> )				
	Paritaprevir	Ritonavir	Ombitasvir	Dasabuvir	M1
CYP3A4	15 / 31%	23 / 83%	~1 / <1%	1.8 / 3.5%	0.5 / <1%

<sup>\*</sup>Paritaprevir, ritonavir, dasabuvir, and M1 data from 10  $\mu$ M incubations; ombitasvir data from 3  $\mu$ M incubations due to low aqueous solubility. Positive controls: 50  $\mu$ M Omeprazole (CYP1A2), 50  $\mu$ M Phenytoin (CYP2B6), 10  $\mu$ M Rifampicin (CYP3A4).

Supplemental Figure 1. PBPK Model Verification of Paritaprevir Simulated PK profile



Supplemental Figure 2. PBPK Model Verification of Ritonavir Simulated PK profile



Supplemental Figure 3. PBPK Model Verification of Dasabuvir Simulated PK profile

